

Exposure Fusion: A Simple and Practical Alternative to High Dynamic Range Photography

T. Mertens¹, J. Kautz² and F. Van Reeth¹

¹Hasselt University — EDM transnationale Universiteit Limburg, Belgium
tom.mertens@uhasselt.be

²University College London, UK

Abstract

We propose a technique for fusing a bracketed exposure sequence into a high quality image, without converting to High dynamic range (HDR) first. Skipping the physically based HDR assembly step simplifies the acquisition pipeline. This avoids camera response curve calibration and is computationally efficient. It also allows for including flash images in the sequence. Our technique blends multiple exposures, guided by simple quality measures like saturation and contrast. This is done in a multiresolution fashion to account for the brightness variation in the sequence. The resulting image quality is comparable to existing tone mapping operators.

Keywords: high dynamic range photography, image fusion, image pyramids

ACM CCS: I.4.8 [Image Processing]: Scene Analysis – Photometry, Sensor Fusion

1. Introduction

Digital cameras have a limited dynamic range, which is lower than one encounters in the real world. In high dynamic range (HDR) scenes, a picture will often turn out to be under- or overexposed. A bracketed exposure sequence [DM97, MP95, RWPD05] allows for acquiring the full dynamic range, and can be turned into a single HDR image. Upon display, the intensities need to be remapped to match the typically low dynamic range of the display device, through a process called tone mapping [RWPD05].

In this paper, we propose to skip the step of computing a HDR, and immediately *fuse the multiple exposures into a high-quality, low dynamic range image, ready for display* (like a tone-mapped picture). We call this process *exposure fusion*; see Figure 2. The idea behind our approach is that we compute a perceptual quality measure for each pixel in the multi-exposure sequence, which encodes desirable qualities, like saturation and contrast. Guided by our quality measures, we select the ‘good’ pixels from the sequence and combine them into the final result.

Exposure fusion is similar to other image fusion techniques for depth-of-field extension [OABB85] and photomontage [ADA*04]. Burt *et al.* [BHK93] have proposed the idea of fusing a multi-exposure sequence, but in the context of general image fusion. We introduce a method that can more easily incorporate desired image qualities, in particular those that are relevant for combining different exposures.

Exposure fusion has several advantages. First of all, the acquisition pipeline is simplified, no in-between HDR image needs to be computed. Since our technique is not physically based, we do not need to worry about calibration of the camera response curve, and keeping track of each photograph’s exposure time. We can even add a flash image to the sequence to enrich the result with additional detail. Our approach merely relies on simple quality measures, like saturation and contrast, which prove to be very effective. Also, results can be computed at near-interactive rates, as our technique mostly relies a pyramidal image decomposition. On the downside, we cannot extend the dynamic range of the original pictures, but instead we directly produce a well-exposed image for display purposes.

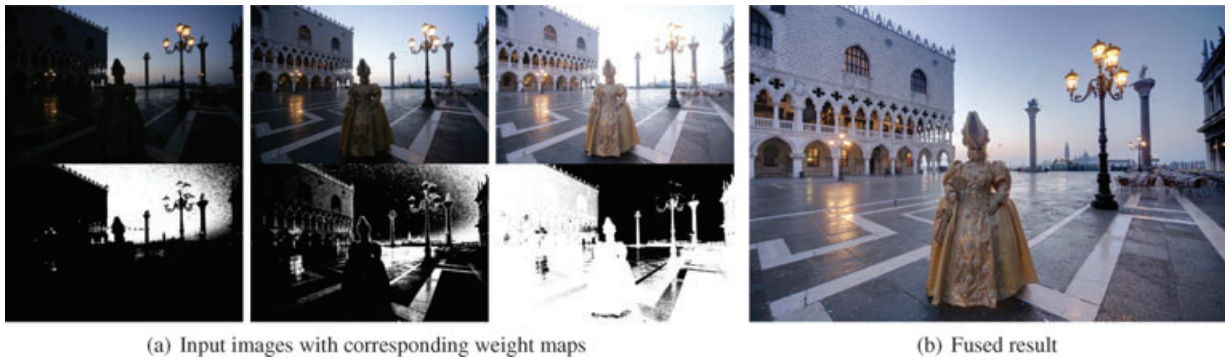


Figure 1: Exposure fusion is guided by weight maps for each input image. A high weight means that a pixel should appear in the final image. These weights reflect desired image qualities, such as high contrast and saturation. Image courtesy of Jacques Joffre.



Figure 2: Demonstration of exposure fusion. A multi-exposure sequence is assembled directly into a high-quality image, without converting to HDR first. No camera-specific knowledge, such as the response curve, had to be accounted for. Total processing time was only 3.3 seconds (1 megapixel). Image courtesy of Jacques Joffre.

2. Related Work

HDR imaging assembles a HDR image from a set of low dynamic range images that were acquired with a normal camera [DM97, MP95]. The camera-specific response curve should be recovered in order to linearize the intensities. This

calibration step can be computed from the input sequence and their exposure settings.

Most display devices have a limited dynamic range and cannot directly display HDR images. To this end, *tone mapping* compresses the dynamic range to fit the dynamic range of the display device [RWPD05]. Many different tone mapping operators have been suggested with different advantages and disadvantages. Global operators apply a spatially uniform remapping of intensity to compress the dynamic range [DMAC03, LRP97, RD05]. Their main advantage is speed, but sometimes fail to reproduce a pleasing image. Local tone mapping operators apply a spatially varying remapping [DW00, DD02, FLW02, LSA05, RSSF02, TR93], i.e. the mapping changes for different regions in the image. This often yields more pleasing images, even though the result may look unnatural sometimes. The operators employ very different techniques to compress the dynamic range: from bilateral filtering [DD02], which decomposes the image into edge-aware low- and high-frequency components, to compression in the gradient domain [FLW02]. The following two local operators are related to our method. Reinhard *et al.* [RSSF02] compute a multi-scale measure that is related to contrast and rescales the HDR pixel values accordingly. This is in a way similar to our measures. However, our measures are solely defined per pixel. The method by Li *et al.* [LSA05] uses a pyramidal image decomposition, and attenuates the coefficients at each level to compress the dynamic range. Our method is also pyramid-based, but it works on the coefficients of the different exposures instead of those of an in-between HDR image. Other tone mappers try to mimic the human visual system, e.g., to simulate temporal adaptation [PTYG00]. Instead, we aim at creating pleasing images and try to reproduce as much detail and colour as possible.

Image fusion techniques have been used for many years. For example, for depth-of-field enhancement [OABB85,

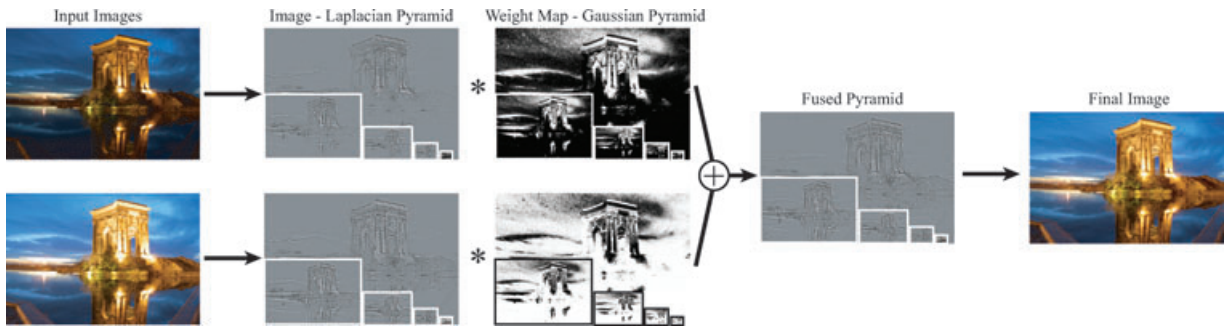


Figure 3: We fuse differently exposed images using a Laplacian decomposition of the images and a Gaussian pyramid of the weight maps, which represent measures such as contrast and saturation. Image courtesy of Jacques Joffre.



Figure 4: Weighted blending. The input sequence is shown in (a). Naive per-pixel blending (b) yields obvious seams due to sharp variations in the weight map. Blurring the weight map using a Gaussian kernel (c) removes the seams, but introduces halos around edges. Cross-bilateral filtering (d) is able to avoid some of the halos, but not all. Multiresolution blending (e) creates the desired result.

Hae94], multimodal imaging [BHK93], and video enhancement [RIY04]. We will use image fusion for creating a high-quality image from bracketed exposures. In the early 1990s, Burt *et al.* [BHK93] have already proposed to use image fusion in this context. However, our method is more flexible by incorporating adjustable image measures, such as contrast and saturation. Goshtasby [Gos05] also proposed a method to blend multiple exposures, but it cannot deal well with object

Figure 5: Comparison with other pyramid-based fusion techniques [OABB85, BHK93]. These methods select the most salient Laplacian pyramid coefficients in the input sequence (a), whereas our technique does blending. The results (b,c) are too dark, and exhibit colour shifts. Our technique (e) produces a more faithful result compared to the input sequence (a). Image courtesy of Jesse Levinson.

boundaries. A more thorough discussion of these techniques is presented in Section 3.3.

Grundland *et al.* [GVWD06] cross-dissolve between two images using a pyramid decomposition [BA83a]. We use a similar blending strategy, but employ different quality measures.

We demonstrate that our technique can be used as a simple way to fuse flash/no-flash images. Previous techniques for this are much more elaborate [ED04, ARNL05] and are specifically designed for this case, whereas our method is flexible enough to handle that case as well.

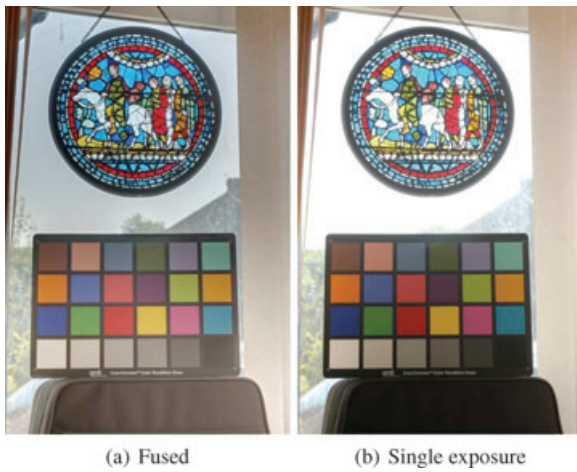


Figure 6: A spurious low-frequency change in brightness might occur due to the difference in exposure among the input images. The result (a) appears too bright towards the bottom, which seems unnatural compared to the input images. One of the input images is shown in (b) for reference.

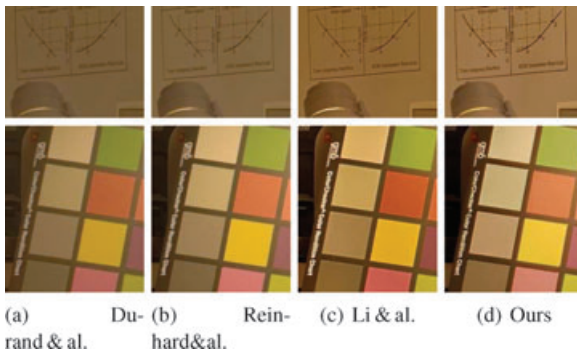


Figure 7: Comparison with several tone mapping techniques: closeups from Figure 8. The results produced by our algorithm exhibit high contrast and good colour reproduction.

3. Exposure Fusion

Exposure fusion computes the desired image by keeping only the ‘best’ parts in the multi-exposure image sequence. This process is guided by a set of quality measures, which we consolidate into a scalar-valued weight map (see Figure 1). It is useful to think of the input sequence as a stack of images. The final image is then obtained by collapsing the stack using **blending**.

As with previous HDR acquisition approaches [MP95, DM97], we assume that the images are perfectly aligned, possibly using a registration algorithm [War03].

3.1. Quality Measures

Many images in the stack contain flat, colourless regions due to under- and overexposure. Such regions should receive less weight, while interesting areas containing bright colours and details should be preserved. We will use the following measures to achieve this:

- **Contrast:** we apply a Laplacian filter to the greyscale version of each image, and take the absolute value of the filter response [MP90]. This yields a simple indicator C for contrast. It tends to assign a high weight to important elements such as edges and texture. A similar measure was used for multi-focus fusion for extended depth-of-field [OABB85].
- **Saturation:** As a photograph undergoes a longer exposure, the resulting colours become desaturated and eventually clipped. Saturated colours are desirable and make the image look vivid. We include a saturation measure S , which is computed as the standard deviation within the R, G and B channel, at each pixel.
- **Well-exposedness:** Looking at just the raw intensities within a channel, reveals how well a pixel is exposed. We want to keep intensities that are not near zero (underexposed) or one (overexposed). We weight each intensity i based on how close it is to 0.5 using a Gauss curve: $\exp\left(-\frac{(i-0.5)^2}{2\sigma^2}\right)$, where σ equals 0.2 in our implementation. To account for multiple colour channels, we apply the Gauss curve to each channel separately, and multiply the results, yielding the measure E .

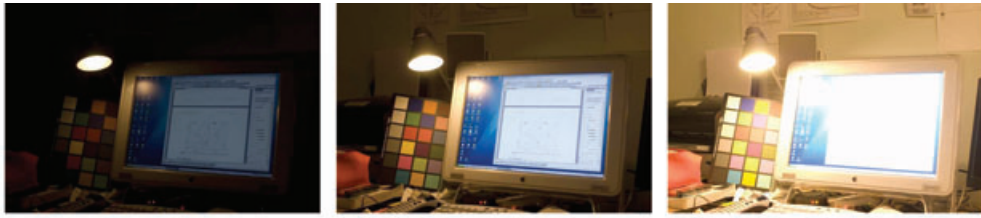
For each pixel, we combine the information from the different measures into a scalar weight map using multiplication. We opted for a product over a linear combination, as we want to enforce all qualities defined by the measures at once (i.e. like an ‘AND’ selection, as opposed to an ‘OR’ selection, respectively). Similar to weighted terms of a linear combination, we can control the influence of each measure using a power function:

$$W_{ij,k} = (C_{ij,k})^{\omega_C} \times (S_{ij,k})^{\omega_S} \times (E_{ij,k})^{\omega_E}$$

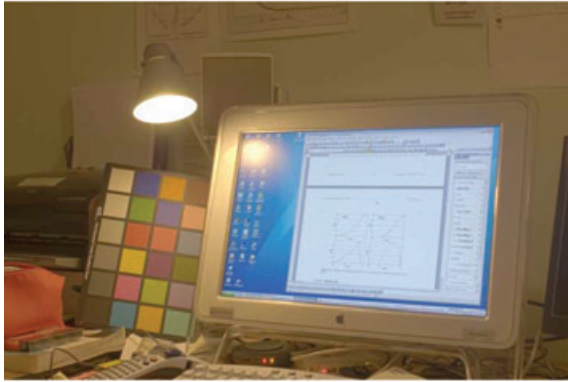
with C , S and E , being contrast, saturation, and well-exposedness, respectively, and corresponding ‘weighting’ exponents ω_C , ω_S and ω_E . The subscript ij, k refers to pixel (i, j) in the k -th image. If an exponent ω equals 0, the corresponding measure is not taken into account. The final pixel weight $W_{ij,k}$ will be used to guide the fusion process, discussed in the next section. See Figure 1 for an example of weight maps.

3.2. Fusion

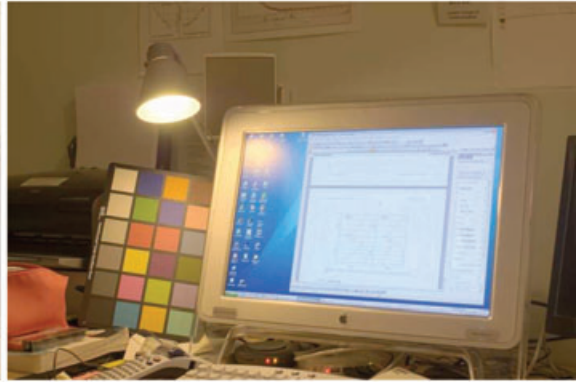
We will compute a weighted average along each pixel to fuse the N images, using weights computed from our quality



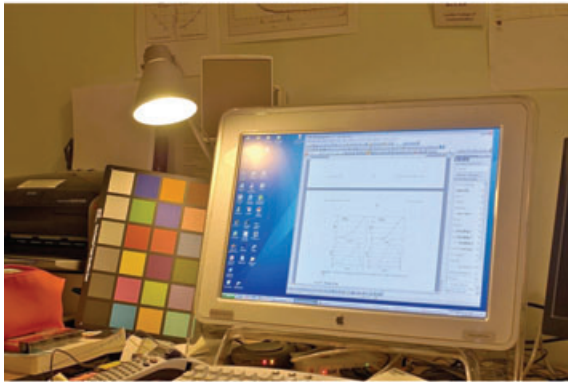
(a) input images



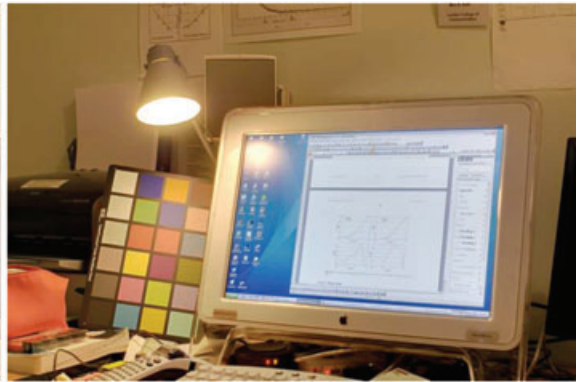
(b) Durand et al. [DD02]



(c) Reinhard et al. [RSSF02]



(d) Li et al. [LSA05]



(e) Our technique

Figure 8: Comparison with several popular tone mapping techniques. Our algorithm yields image quality that is competitive with the other results. See Figure 7 for a more detailed inspection.

measures. To obtain a consistent result, we normalize the values of the N weight maps such that they sum to one at each pixel (i, j) :

$$\hat{w}_{ij,k} = \left[\sum_{k'=1}^N w_{ij,k'} \right]^{-1} w_{ij,k}.$$

The resulting image R can then be obtained by a weighted blending of the input images:

$$R_{ij} = \sum_{k=1}^N \hat{w}_{ij,k} I_{ij,k} \quad (1)$$

with I_k the k -th input image in the sequence. Unfortunately, just applying Equation (1) produces an unsatisfactory result. Wherever weights vary quickly, disturbing seams will appear (Figure 4b). This happens because the images we are combining, contain different absolute intensities due to their different exposure times. We could avoid sharp weight map transitions by smoothing the weight map with a Gaussian filter, but this results in undesirable halos around edges, and spills information across object boundaries (Figure 4c). An edge-aware smoothing operation using the cross-bilateral filter seems like a better alternative [PSA*04, ED04]. However, it is unclear how to define the control image, which would tell us where the smoothing should be stopped. Using the



Figure 9: Combining a flash/no-flash image pair using our technique. Notice how the highlight is removed, while detail and contrast has been transferred to the face. Images taken from Agrawal et al. [ARNL05].

original greyscale image as control image does not work well, as demonstrated in Figure 4d. Also, it is hard to find good parameters for the cross-bilateral filter (i.e. for controlling the spatial and intensity influence).

To address the **seam** problem, we use a technique inspired by Burt and Adelson [BA83b]. Their original technique seamlessly blends two images, guided by an alpha mask, and works at multiple resolutions using a pyramidal image decomposition. First, the input images are decomposed into a Laplacian pyramid, which basically contains band-pass filtered versions at different scales [BA83a]. Blending is then carried out for each level separately. We adapt the technique to our case, where we have N images and N normalized weight maps that act as alpha masks. Let the l -th level in a Laplacian pyramid decomposition of an image A be defined as $\mathbf{L}\{A\}^l$, and $\mathbf{G}\{B\}^l$ for a Gaussian pyramid of image B . Then, we blend the coefficients (pixel intensities in the different pyramid levels) in a similar fashion to Equation (1):

$$\mathbf{L}\{R\}_{ij}^l = \sum_{k=1}^N \mathbf{G}\{\hat{W}\}_{ij,k}^l \mathbf{L}\{I\}_{ij,k}^l.$$

Thus, each level l of the resulting Laplacian pyramid is computed as a weighted average of the original Laplacian decompositions for level l , with the l -th level of Gaussian pyramid of the weight map serving as the weights. **Finally, the pyramid $\mathbf{L}\{R\}^l$ is collapsed to obtain R .** An overview of our technique is given in Figure 3.

Multiresolution blending is quite effective at avoiding seams (Figure 4), because it blends image features instead of intensities. Since the blending Equation (1) is computed at each scale separately, sharp transitions in the weight map can only affect sharp transitions that appear in the original images (e.g. edges). Conversely, flat regions in the original images will always have negligible coefficient magnitude, and are thus not affected by possibly sharp variations in the weight function, even though the absolute intensities among the inputs could be different there.

For dealing with colour images, we have found that carrying out exposure fusion in each colour channel separately produces good results.

3.3. Discussion

Seamless blending is an often-encountered problem in image processing and graphics. We use a multiresolution technique based on image pyramids [BA83b], but other methods are available as well. In particular, gradient-based blending [PGB03] has shown to be effective, and it has been applied to image fusion as well [ADA*04, RIY04]. Gradient methods convert images to gradient fields first, apply the blending operation, and reconstruct the final image from the resulting gradients. However, reconstruction requires solving a partial differential equation, which can be costly for high-resolution



Figure 10: Comparison of our quality measures. Exposure fusion is performed with each measure turned on separately. See Section 4.4 for a discussion. Bottom images courtesy of Jacques Joffre.

images. In addition, gradient-based fusion incurs a scale and shift ambiguity, and is prone to colour shifting [RIY04].

Tone mapping operators may also cause colour shifts like oversaturation [LSA05], and possibly reduce contrast (see Figure 8). Our blending is robust against changes in appearance, as it can be seen as a selection process. Even though we select based on contrast and saturation, we do not directly change pixels to meet these constraints.

Our work bears similarity to early work on image fusion, where the Laplacian (or another) pyramid decomposition is used as well [OABB85, Toe90, BHK93]. These methods work directly on the coefficients by retaining only those pyramid coefficients that are most salient. For instance, the coefficients with the largest magnitude are kept [OABB85]:

$$\mathbf{L}\{R\}_{ij}^l = \underset{\mathbf{L}\{I\}_{ij,k}^l}{\operatorname{argmax}} |\mathbf{L}\{I\}_{ij,k}^l|$$

Burt and Kolczynski's exposure fusion technique [BHK93] is based on the same principle. These approaches compound all details present in the sequence, but they do

not necessarily produce an appealing result; see Figure 5. Instead, we blend the pyramid coefficients based on a scalar weight map, but do not directly process individual coefficients at different levels. Measures like saturation and well-exposedness are hard to evaluate directly from pyramid coefficients. Our technique basically decouples the weighting from the actual pyramid contents, which enables us to more easily define quality measures. In fact, any measure that can be computed per-pixel, or perhaps in a very small neighbourhood, is applicable. Alternatively, we could also compute the measures (and thus the weights) at multiple resolutions in a Gaussian pyramid decomposition of the input images. However, this would increase the computational cost, as more pixels need to be weighted, while the benefit remains unclear.

Goshtasby's technique [Gos05] selects the optimal exposure on a per-block basis, and smoothly blends between blocks. Since blocks may overlap with different objects, information will spill over object boundaries, similar to the artifacts related to Gaussian blurring of the weight map (Figure 4c).

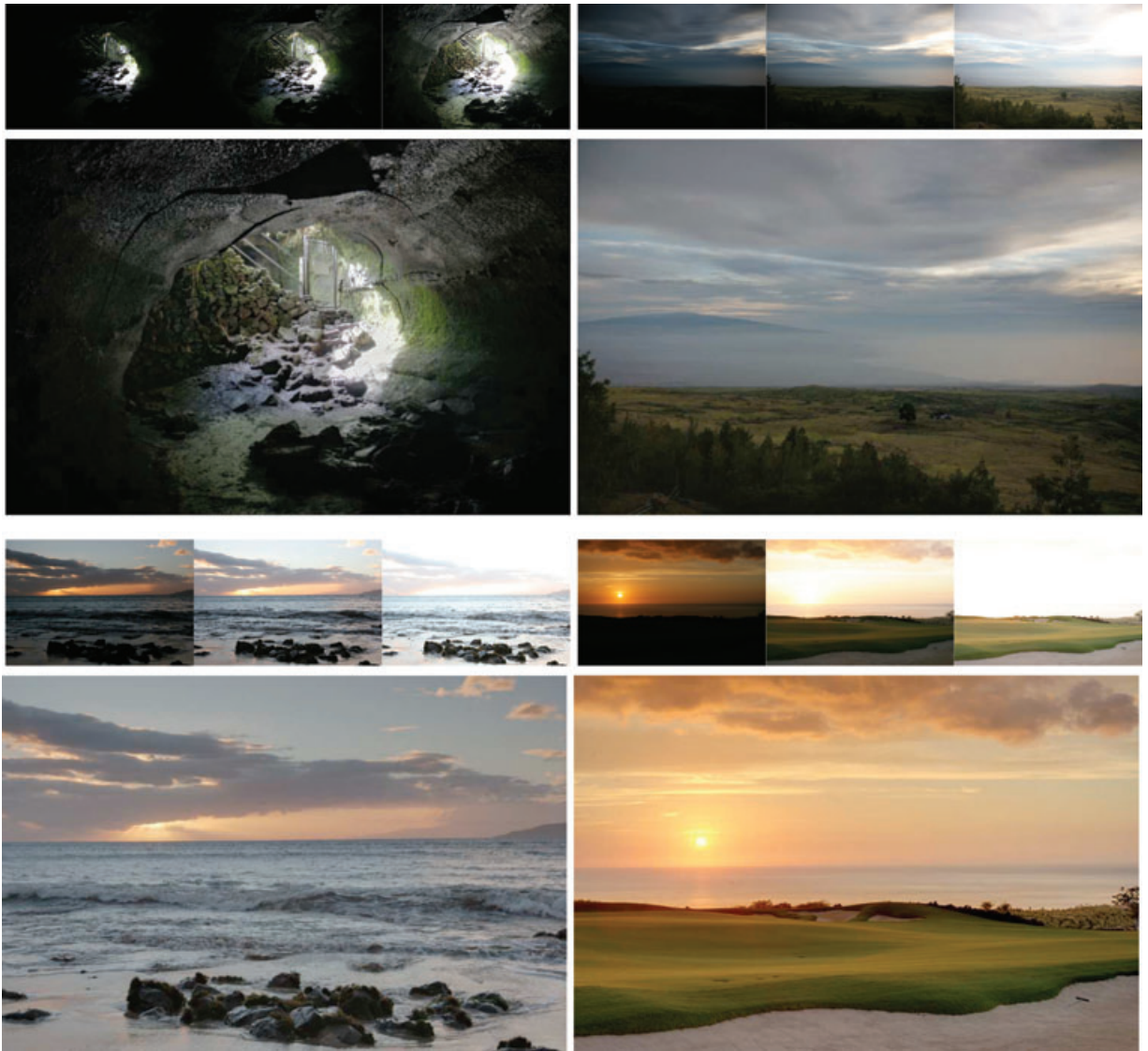


Figure 11: More examples. The input images are shown as thumbnails above each result. Note how each image captures all details from the input sequence. Bottom right image courtesy of Jesse Levinson.

4. Results

All of our examples were constructed from JPG-encoded photographs, with unknown gamma correction and camera response curve. We used equally weighted quality measures ($\omega_C = \omega_S = \omega_E = 1$) in most examples, except where mentioned otherwise.

4.1. Quality

Figures 2 and 1 show a typical bracketed exposure shot: underexposed, normally exposed and overexposed. Every ex-

posure contains relevant information that is not present in the other exposures. Our technique is able to preserve finescale details of the buildings, and the warm appearance of the sky. More results can be found in Figure 11.

In Figures 8 and 7, we compare our result to tone mapping. A rigorous comparison is hard, due to the operators' implementation-specific differences and parameter settings. We therefore limit ourselves to an informal comparison with a few popular tone mappers. Compared to Durand and Dorsey [DD02] and Reinhard *et al.* [RSSF02], our method offers better contrast. Li *et al.*'s approach [LSA05] produces quite similar results to ours in terms of

Table 1: Computation times for our technique. We computed re-sults for $\frac{1}{2}$, 1 and 2 megapixel images. N is the number of images in the stack. The initialization builds the Laplacian pyramids for each input image. The update step computes the weight maps, the corresponding Gaussian pyramids and the blending. For small image sizes (half to one megapixel), the user gets interactive interactive feedback (about 1 second).

$w \times h \times N$	init. (s)	update (s)	total (s)
$864 \times 576 \times 3$	0.75	0.82	1.6
$1227 \times 818 \times 3$	1.5	1.6	3.2
$1728 \times 1152 \times 3$	3.0	3.2	6.2
$864 \times 576 \times 7$	1.5	1.5	3.0
$1227 \times 818 \times 7$	3.0	3.1	6.1
$1728 \times 1152 \times 7$	6.0	6.0	12.0

contrast, but it also exhibits slight oversaturation. We had to tweak the saturation parameter in their implementation to correct the colours.

The multiresolution blending technique discussed in Section 3.2 is not without its problems. In Figure 6, our result contains a spurious low frequency brightness change, which is not present in the original image set. It is caused by a highly varying change in brightness among the different exposures. Intuitively speaking, this artifact can be considered as a very blurred version of the seam problem, illustrated in Figure 4b. Constructing a higher Laplacian pyramid partially solves this problem. However, the pyramid height is also limited by the size of the downsampling/upsampling filter [BA83a].

Another issue concerns out-of-range artifacts. The pyramid reconstruction does not guarantee that the resulting intensities lie within $[0, 1]$, even if the original intensities were restricted to this domain. E.g. in Figure 8, the area below the monitor has become overly dark as the intensities fall below 0. One can simply fix this issue by shifting and scaling the intensities, at the risk of reducing contrast.

4.2. Performance

Our unoptimised software implementation performs exposure fusion in a matter of seconds; see Table 1. After building the Laplacian pyramids, our technique can provide near-interactive feedback (see timings of update step). This enables a user gain more control over the fusion process, as he or she can adjust the weighting of quality measures. Additional controls on the input images, such as linear and non-linear intensity remappings are also possible (like brightness adjustment or gamma curves). This can be used to give certain exposures more influence. Motivated by the work of Strengert *et al.* [SKE06], we expect that our algorithm could eventually run in real time on graphics hardware.

4.3. Including Flash-Exposures

A flash exposure can fill in a lot of detail, but tends to produce unappealing images, and it may include spurious highlights and reflections. Recent work on flash photography has introduced techniques for combining flash/no-flash image pairs [ED04, PSA*04, ARNL05]. Our technique can be used here as well, as our quality measures are also relevant in this case. Figure 9 shows how our technique has successfully removed a highlight and filled in details, similar to Agrawal *et al.* [ARNL05]. However, it cannot remove flash shadows [ED04] or unwanted reflections [ARNL05]. We used the contrast measure for these examples ($\omega_C = 1$ and $\omega_S = \omega_E = 0$).

4.4. Comparison of Quality Measures

Figure 10 shows a comparison of our quality measures. Exposure fusion is performed with either contrast, saturation or well-exposedness. The desk scene in the first row comes out better with saturation turned on. Contrast makes the background a bit dark, and well-exposedness darkens the centre of the monitor, making the result look unnatural. For the house scene on the next row, saturation and well-exposedness produce vivid colours, which is less so for contrast. Finally, the last row shows how contrast retains details, which are not present in the saturation image (e.g. in the water, and the buildings' windows). Well-exposedness yields a more surrealist result.

In general, we found that well-exposedness by itself produces fairly good images. However, in some cases it tends to create an unnatural appearance, because it always favours intensities around 0.5. Saturation and contrast does not have this problem. But then again, the results from those measures are not always as interesting as those produced by well-exposedness.

5. Conclusion

We proposed a technique for fusing a bracketed exposure sequence into a high-quality image, without converting to HDR first. Skipping the physically based HDR assembly step simplifies the acquisition pipeline. It avoids camera response curve calibration, it is computationally efficient, and allows for including flash images in the sequence. Our technique blends images in a multi-exposure sequence, guided by simple quality measures like saturation and contrast. This is done in a multiresolution fashion to account for the brightness variation in the sequence. Quality is comparable to existing tone mapping operators. Our approach is controlled by only a few intuitive parameters, which can be updated at near-interactive rates in our unoptimised implementation.

We would like to investigate different pyramidal image decompositions, such as wavelets and steerable pyramids. Also, we would like to include more measures, in particular

one that would detect camera noise. An optimised Graphics Processing Unit (GPU) implementation would enable the user to interactively control the fusion process, but could also be used to display a multi-exposure video stream [MMC*07] in real time. Finally, we would like to look into the applicability of our technique to other image fusion tasks, such as depth-of-field extension [OABB85] and multimodal imaging [BHK93].

Acknowledgments

Thanks to Jacques Joffre, Jesse Levinson, Min H. Kim and Agrawal *et al.* [ARNL05] for sharing their photographs. Part of the research at Expertise Centre for Digital Media (EDM) is funded by the European Regional Development Fund.

References

- [ADA*04] AGARWALA A., DONTCHEVA M., AGRAWALA M., DRUCKER S. M., COLBURN A., CURLESS B., SALESIN D. and COHEN M. F.: Interactive digital photomontage. *ACM Trans. Graph* 23, 3 (2004), 294–302.
- [ARNL05] AGRAWAL A., RASKAR R., NAYAR S. K. and LI Y.: Removing photography artifacts using gradient projection and flash-exposure sampling. *ACM Trans. Graph.* 24, 3 (2005), 828–835.
- [BA83a] BURT P. and ADELSON T.: The Laplacian Pyramid as a Compact Image Code. *IEEE Transactions on Communication COM-31* (1983a), 532–540.
- [BA83b] BURT P. J. and ADELSON E. H.: A multiresolution spline with application to image mosaics. *ACM Transactions on Graphics* 2 (October 1983), 217–236.
- [BHK93] BURT P. J., HANNA K. and KOLCZYNSKI R. J.: Enhanced image capture through fusion. In *Proceedings of the Workshop on Augmented Visual Display Research* (December 1993), NASA – Ames Research Center, pp. 207–224.
- [DM97] DEBEVEC P. E. and MALIK J.: Recovering high dynamic range radiance maps from photographs. In *SIGGRAPH '97: Proceedings of the 24th annual conference on Computer graphics and interactive techniques* (New York, NY, USA, 1997), ACM Press/Addison-Wesley Publishing Co., pp. 369–378.
- [DW00] DiCARLO J. and WANDELL B.: Rendering high dynamic range images. In *Proceedings of SPIE* (January 2000), vol. 3965.
- [DMAC03] DRAGO F., MYSZKOWSKI K., ANNEN T. and CHIBA N.: Adaptive logarithmic mapping for displaying high contrast scenes. *Computer Graphics Forum* 22 (2003), 419–426.
- [DD02] DURAND F. and DORSEY J.: Fast bilateral filtering for the display of high-dynamic-range images. *ACM Trans. Graph* 21, 3 (2002), 257–266.
- [ED04] EISEMANN E. and DURAND F.: Flash photography enhancement via intrinsic relighting. In *ACM Transactions on Graphics (Proceedings of Siggraph Conference)* (2004), vol. 23, ACM Press.
- [FLW02] FATTAL R. and LISCHINSKI D., WERMAN M.: Gradient domain high dynamic range compression. *ACM Transactions on Graphics* 21, 3 (July 2002), 249–256.
- [Gos05] GOSHTASBY A.: Fusion of multi-exposure images. *Image and Vision Computing* 23 (2005), 611–618.
- [GVWD06] GRUNDLAND M., VOHRA R., WILLIAMS G. P. and DODGSON N. A.: Cross dissolve without cross fade: Preserving contrast, color and salience in image compositing. *Computer Graphics Forum* 25, 3 (September 2006), 577–586.
- [Hae94] HAEERLI P.: A multifocus method for controlling depth of field. <http://www.graficaobscura.com/depth/index.html>, 1994.
- [LRP97] LARSON G. W., RUSHMEIER H. E. and PIATKO C. D.: A visibility matching tone reproduction operator for high dynamic range scenes. *IEEE Trans. Vis. Comput. Graph* 3, 4 (1997), 291–306.
- [LSA05] LI Y., SHARAN L. and ADELSON E. H.: Compressing and companding high dynamic range images with sub-band architectures. *ACM Transactions on Graphics* 24, 3 (August 2005), 836–844.
- [MP90] MALIK J. and PERONA P.: Preattentive texture discrimination with early vision mechanism. *Journal of the Optical Society of America* 7, 5 (May 1990), 923–932.
- [MP95] MANN S. and PICARD R.: Being ‘undigital’ with digital cameras: Extending dynamic range by combining differently exposed pictures. In *Proceedings of IS&T 46th annual conference*. (May 1995), pp. 422–428.
- [MMC*07] MCGUIRE M., MATUSIK W., CHEN B., HUGHES J. F., PFISTER H. and NAYAR S.: Optical splitting trees for high-precision monocular imaging. *Computer Graphics and Applications* 27, 2 (March–April 2007), 32–42.
- [OABB85] OGDEN J. M., ADELSON E. H., BERGEN J. R. and BURT P. J.: Pyramid-based computer graphics. *RCA Engineer* 30, 5 (1985).
- [PTYG00] PATTANAIK S. N., TUMBLIN J. E., YEE H. and GREENBERG D. P.: Time-Dependent visual adaptation for realistic Real-Time image display. In *Proceedings of SIGGRAPH 2000* (2000), Computer Graphics Proceedings, Annual Conference Series, pp. 47–54.

- [PGB03] PÉREZ P., GANGNET M. and BLAKE A.: Poisson image editing. In *SIGGRAPH '03: ACM SIGGRAPH 2003 Papers* (New York, NY, USA, 2003), ACM Press, pp. 313–318.
- [PSA*04] PETSCHNIG G., SZELISKI R., AGRAWALA M., COHEN M. F., HOPPE H. and TOYAMA K.: Digital photography with flash and no-flash image pairs. *ACM Trans. Graph* 23, 3 (2004), 664–672.
- [RIY04] RASKAR R., ILIE A. and YU J.: Image fusion for context enhancement and video surrealism. In *Proceedings of the 3rd Symposium on Non-Photorealistic Animation and Rendering* (2004), pp. 85–152.
- [RD05] REINHARD E. and DEVLIN K.: Dynamic range reduction inspired by photoreceptor physiology. *IEEE Trans. Vis. Comput. Graph* 11, 1 (2005), 13–24.
- [RSSF02] REINHARD E., STARK M., SHIRLEY P. and FERWERDA J.: Photographic tone reproduction for digital images. *ACM Transactions on Graphics* 21, 3 (July 2002), 267–276.
- [RWPD05] REINHARD E., WARD G., PATTANAİK S. and DEBEVEC P.: *High Dynamic Range Imaging: Acquisition, Display and Image-Based Lighting*. Morgan Kaufmann Publishers, Los Alamitos, CA, USA, Dec. 2005.
- [SKE06] STRENGERT M., KRAUS M. and ERTL T.: Pyramid Methods in GPU-Based Image Processing. In *Workshop on Vision, Modelling, and Visualization VMV '06* (2006), pp. 169–176.
- [Toe90] TOET A.: Hierarchical image fusion. *Mach. Vision Appl.* 3, 1 (1990), 1–11.
- [TR93] TUMBLIN J., RUSHMEIER H. E.: Tone reproduction for realistic images. *IEEE Computer Graphics and Applications* 13, 6 (November 1993), 42–48.
- [War03] WARD G.: Fast, robust image registration for compositing high dynamic range photographs from hand-held exposures. *Journal of Graphics Tools: JGT* 8, 2 (2003), 17–30.